ACS APPLIED MATERIALS & INTERFACES

www.acsami.org

Research Article

Prototype Design of a Domain-Wall-Based Magnetic Memory Using a Single Layer $La_{0.67}Sr_{0.33}MnO_3$ Thin Film

Shizhe Wu, Yuelin Zhang, Chengfeng Tian, Jianyu Zhang, Mei Wu, Yu Wang, Peng Gao, Haiming Yu, Yong Jiang, Jie Wang,* Kangkang Meng,* and Jinxing Zhang*

Cite This: *ACS Appl. Mater. Interfaces* 2021, 13, 23945−23950

Read Online

ACCESS | Metrics & More | Article Recommendations | Supporting Information

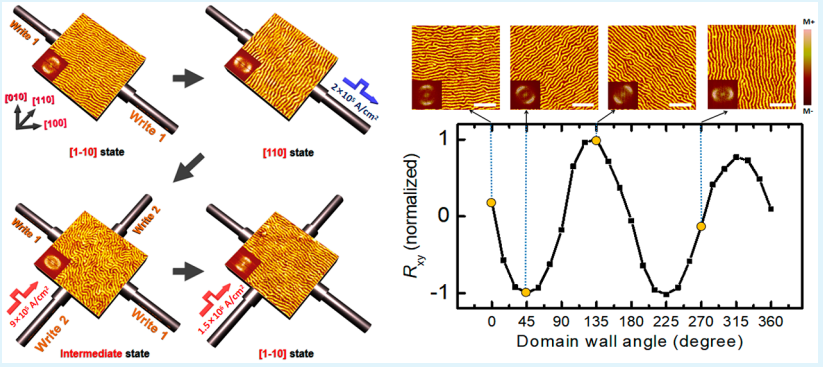

ABSTRACT: Magnetic field-free, nonvolatile magnetic memory with low power consumption is highly desired in information technology. In this work, we report a current-controllable alignment of magnetic domain walls in a single layer $La_{0.67}Sr_{0.33}MnO_3$ thin film with the threshold current density of 2×10^5 A/cm^2 at room temperature. The vector relationship between current directions and domain-wall orientations indicates the dominant role of spin−orbit torque without an assistance of external magnetic field. Meanwhile, significant planar Hall resistances can be readout in a nonvolatile way before and after the domain-wall reorientation. A domain-wall-based magnetic random-access memory (DW-MRAM) prototype device has been proposed.

KEYWORDS: *field-free magnetic switching, magnetic domain wall, oxide materials, spin−orbit coupling, planar hall effect, magnetic random-access memory*

Downloaded via PEKING UNIV on September 4, 2023 at 15:28:17 (UTC).
See https://pubs.acs.org/sharingguidelines for options on how to legitimately share published articles.

INTRODUCTION

Spintronic devices such as giant magnetoresistance (GMR)/magnetic tunnel junction (MTJ)-based hard drives[1] and spin-transfer torque magnetic random-access memory (STT-MRAM)[2] have been already applied in information technology. Recently, spin−orbit torque magnetic random-access memory (SOT-MRAM) shows great potentials in devices with low-power consumption, high writing/reading speed, and high endurance.[3] SOT effect has been discovered in heavy metal/ferromagnet heterostructures, in which the charge current can be converted into spin current due to strong spin−orbit coupling (SOC) of heavy metals or symmetry-broken interfaces, inducing effective torques on the ferromagnets.[4,5] However, traditional SOT devices require an in-plane magnetic field or additional effective fields (antiferromagnetic pinning layer, magnetocrystalline anisotropy, etc.) to deterministically switch the perpendicular magnetization,[6−9] bring a lot of challenges in the integration process of the SOT-MARM.

In order to achieve a simple device design, SOC effective magnetic field can be used to switch the in-plane magnetization.[4] SOT-induced single layer in-plane magnetization switching has been widely studied in a variety of ferromagnetic and antiferromagnetic materials.[10−13] Compared with previous studies on magnetic monodomain switching,[14] the magnetic domain wall (DW)-based structure shows nonvolatile in-plane realignment in a deterministic manner.[15] Ordered stripe DWs can be stabilized in single layer ferromagnetic $La_{0.67}Sr_{0.33}MnO_3$ (LSMO) thin films and realigned by in-plane magnetic field (or effective magnetic field).[16,17] Its DWs orientation is directly related to the in-plane magnetization, which indicates that LSMO could be a candidate for DW-based SOT.

RESULTS AND DISCUSSION

High-quality LSMO thin films with a thickness of 150 nm have been grown by pulsed laser deposition (PLD) on single crystal

Received: March 12, 2021
Accepted: May 5, 2021
Published: May 11, 2021

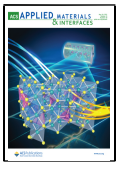

© 2021 American Chemical Society

https://doi.org/10.1021/acsami.1c04724
ACS Appl. Mater. Interfaces 2021, 13, 23945−23950

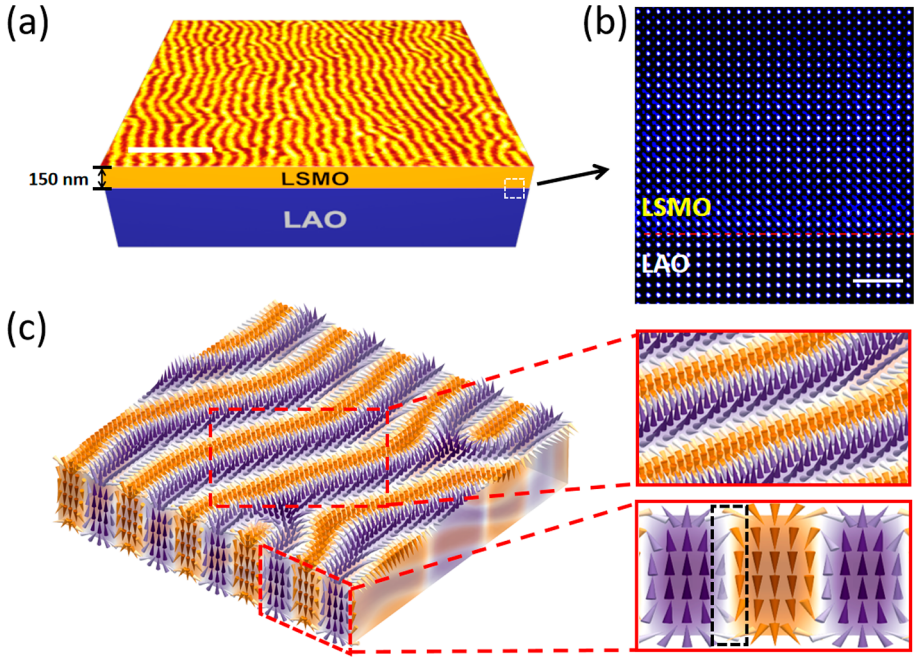

Figure 1. (a) Magnetic domain images of the LSMO thin film with a thickness of 150 nm. The scale bar is 1 μm. (b) High angle annular dark field (HAADF) image shows the interface of LAO substrate and LSMO film. The scale bar is 2 nm. (c) Phase-field simulation of the stripe domain textures. Inside the black square is the vortex-like domain wall.

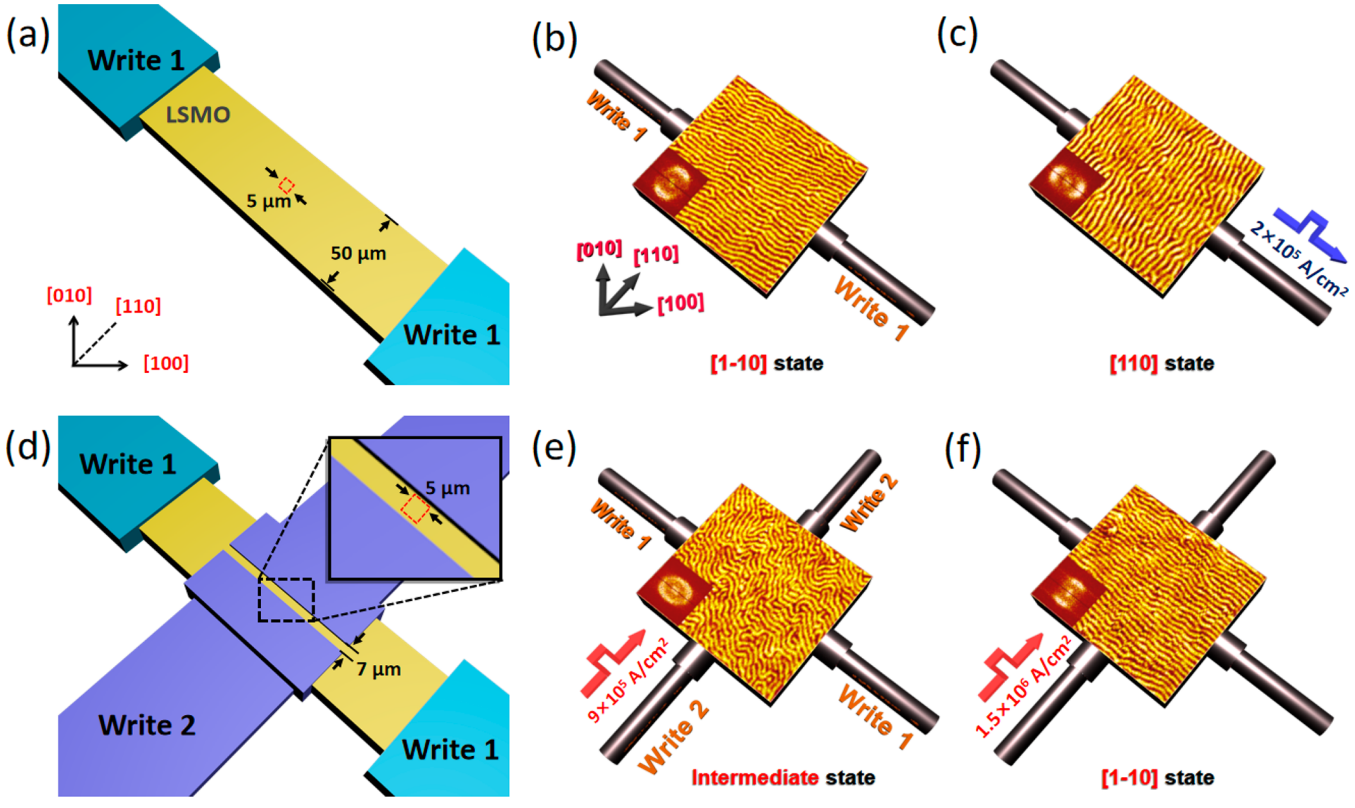

Figure 2. Schematics of the device and magnetic domain images of the current-induced DWs rotation process. (a) The LSMO bar structure and the "write 1" circuit along [1−10] crystal orientation. The MFM images were captured at the red square. (b) The initial stripe DWs along [1−10] crystal orientation. (c) The stripe DWs rotated to [110] crystal orientation after a current pulse applied along [1−10] crystal orientation. (d) The "write 2" circuit with a 7 μm width gap along [110] crystal orientation. (e) The stripe DWs rotated to an intermediate state by a current pulse applied along [110] crystal orientation. (f) The stripe DWs rotated back by a current pulse applied along [110] crystal orientation. The scale size of these MFM images is 5 × 5 μm. The insets show the Fourier transformation images of the corresponding MFM patterns.

$LaAlO_3$ (LAO) (001) substrates. X-ray diffraction (XRD) pattern (Supporting Information (SI) Figure S1) shows that the lattice mismatch between the LSMO and LAO gives rise to in-plane compressive and out-of-plane tensile strains. The

https://doi.org/10.1021/acsami.1c04724
ACS Appl. Mater. Interfaces 2021, 13, 23945−23950

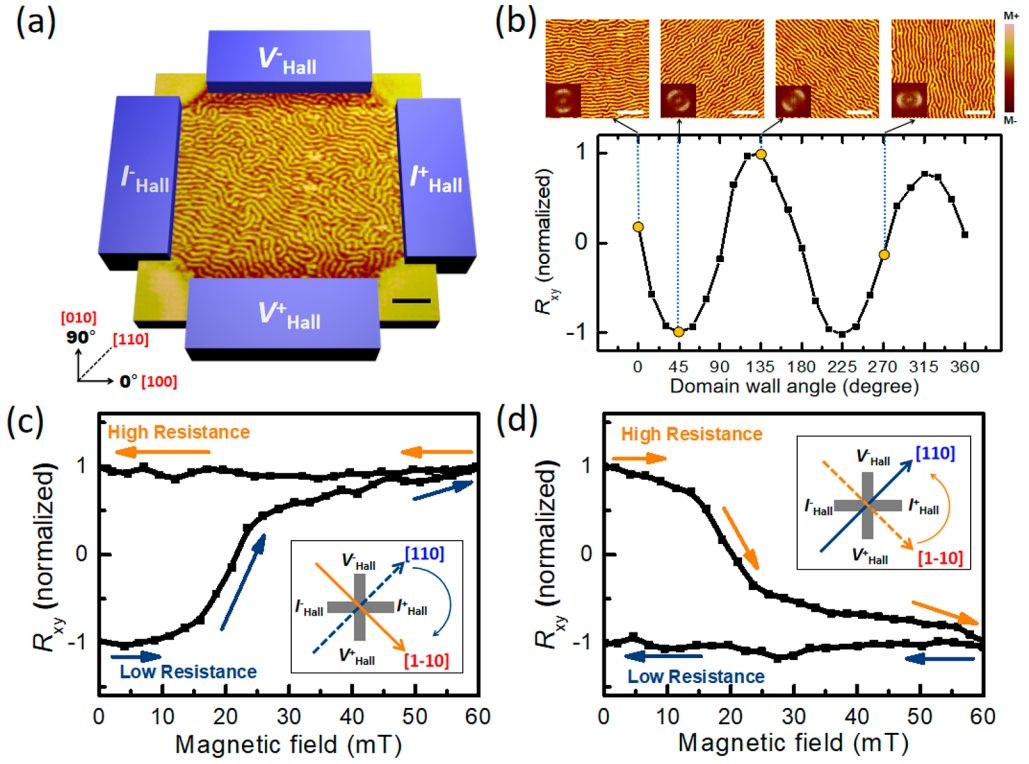

Figure 3. (a) Magnetic domain image and the read circuit of the PHE device. The scale bar is 1 μm. (b) Nonvolatile PHE readout and corresponding magnetic domain images along different orientations. The MFM picture and planar Hall resistance are captured/measured at room temperature at zero magnetic field. The insets show the Fourier transformation images of the corresponding MFM patterns. The scale bar is 1 μm. (c) Magnetic-field dependence of the nonvolatile Hall resistance R_{xy}. The gray arrows indicate loop process from low resistance to high resistance states. Inset picture shows the magnetic field and the original magnetization direction. (d) The opposite process from high resistance to low resistance states.

ferromagnetic properties of the LSMO thin films have been discussed previously.[17,18] The magnetic domain image of the LSMO thin film was captured by magnetic force microscopy (MFM) at room temperature and zero magnetic field (Figure 1a), which shows the stripe domain feature with out-of-plane upward (bright stripes) and downward (dark stripes) magnetizations. The high-quality epitaxial interface has been characterized by high angle annular dark field (HAADF) scanning transmission electron microscopy (STEM) in Figure 1b. Detailed spin textures of the stripe domains are shown in Figure 1c by the phase field simulation. The cross-sectional DW structure can be consisted by the Néel type at the top/bottom regions and the Bloch type at the center, forming a vortex-like spin texture.[19] Such stripe domain can be easily reoriented under in-plane magnetic field due to the in-plane spin orientation of the vortex-like core.[15]

Figure 2 shows the experimental geometry of the current-induced DWs rotation in LSMO. First, only the "write 1" electrodes were fabricated on the bar structure of LSMO thin film along [1−10] crystal orientation (Figure 2a). The stripe DWs were initialized along [1−10] crystal orientation by magnetic field (about 100 mT for fully saturation, then removed the magnetic field) as shown in Figure 2b. When a 10-μs-width pulsed current with 2×10^5 A/cm^2 density was applied along [1−10] crystal orientation, the stripe DWs were rotated to [110] crystal orientation (Figure 2c). Second, we fabricated the "write 2" electrodes on the bar structure (Figure 2d) in order to apply a current along [110] crystal orientation. When a pulsed current of9×10^5 A/cm^2 was applied along [110] crystal orientation, the stripe DWs could not be rotated by 90 deg but formed an intermediate state (Figure 2e). The stripe DWs can be rotated by 90 deg to [1−10] crystal orientation when the current density reaches 1.5×10^6 A/cm^2 (Figure 2f).

The different in-plane magnetic anisotropy energies of LSMO thin film along two crystal orientations explain the different current densities between two crystal orientations.[20] Moreover, the possible thermal effect has been further analyzed in SI Figure S2. However, these current-induced realignment behaviors are highly dependent on the orientation of the current and exhibit an intermediate state, which cannot be explained only by the thermal effect or Oersted field. In single layer LSMO film, SOC can be generated by strain-induced inversion asymmetry from the substrate. The direction of the SOC effective magnetic field is perpendicular to the current along [110] (or [−1−10]) and [1−10] (or [−110]) crystal orientations,[4,5,10] which has been qualitatively discussed[21] in SI Figures S3 and S4. For the above reasons, we speculate that our current-induced domain-wall reorientation is a SOT effect. However, STT effect can also contribute when current is driven through the domain texture. The current-induced domain wall motion has been observed due to vertical spin-transfer torque by a probe-based technique in our previous reports in reference.[18,22] The interaction between the STT effect with the complex (Neel/Bloch) domain walls structure is lack of analysis. Further in-depth research is needed to clear the mechanism of this current induced magnetic switching.

To readout DW states, we chose the planar Hall effect (PHE) which is mainly derived from in-plane magnetic

https://doi.org/10.1021/acsami.1c04724
ACS Appl. Mater. Interfaces 2021, 13, 23945−23950

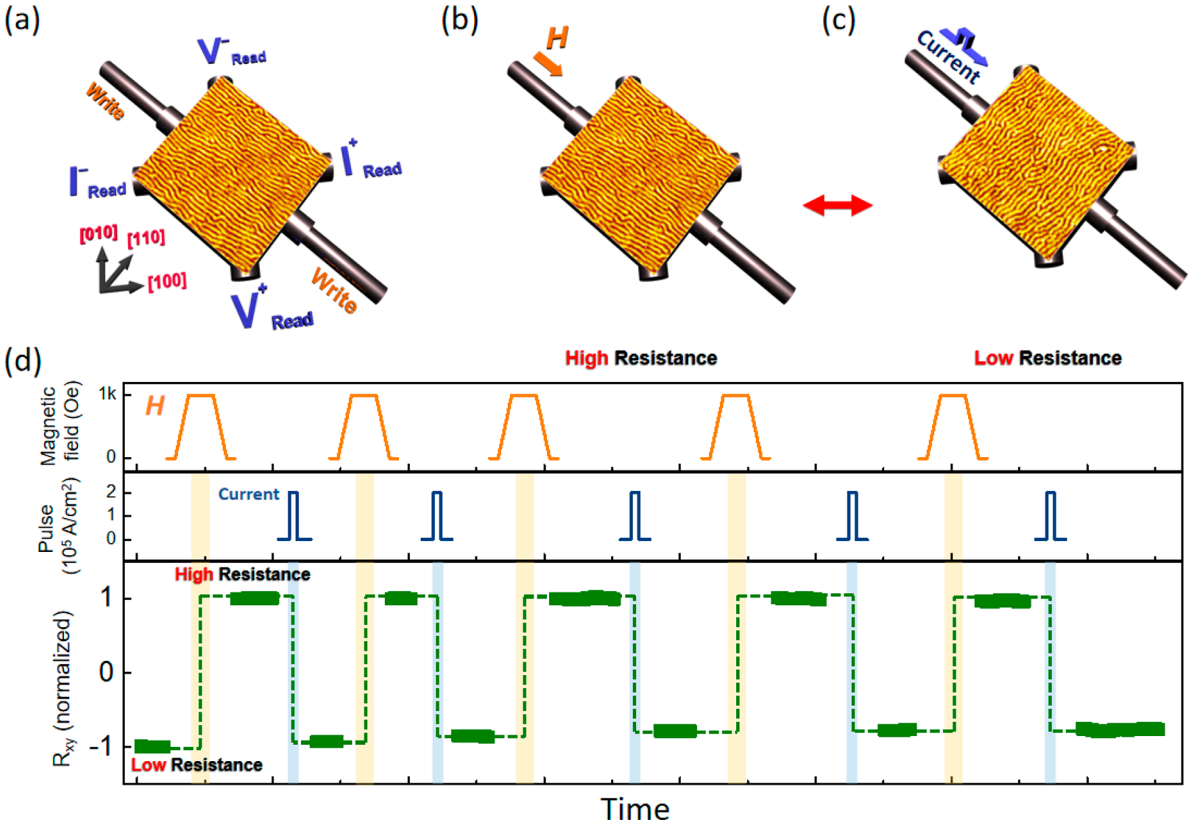

Figure 4. (a) Schematics of the device six electrodes device with an in-plane pulse magnetic field to simulate the electrodes along [110] crystal orientation. Single LSMO thin film is used as magnetic memory cell. Blue and orange labeled electrodes indicate read and write circuits. (b) High resistance ([1−10]) state of the DW-MARM induced by in-plane magnetic field along [1−10] crystal orientation. (c) Low resistance ([110]) state of the DW-MARM induced by current pulse of 2×10^5 A/cm^2 along [1−10] crystal orientation. (d) Current/field combined repeatable nonvolatile switching of the high ([1−10]) and low ([110]) PHE resistance states.

anisotropy.[23,24] PHE has many advantages such as high signal/noise ratio and low thermal drift.[25] Figure 3a shows the read circuit of the PHE and the relationship between the rotation angle and the crystal orientations. The PHE (normalized Hall resistance R_{xy}) at different orientations of the stripe DWs are shown in Figure 3b. The stripe DWs were rotated to each specific angle by a magnetic field of about 100 mT, then the magnetic field was removed. The MFM pictures and planar Hall resistances were captured/measured at room temperature at zero magnetic field. The resistance difference ΔR_{xy} is about 0.02 Ω. The calculated resistivity change $\Delta\rho_{xy}$ is about 0.3 μΩ cm, at the same order of magnitude of the reported PHE-single-layer-SOT device.[11] The rotation-angle-dependent Hall resistance value shows a period of 180°. The R_{xy} are not the same at 135° and 315° which may be due to the misalignment of the sample rotator. However, in contrast to the DW magnetoresistance effect,[22] the valley and peak are at 45° and 135°, which is an obvious characteristic of PHE. We verified the nonvolatility of the DW rotation through the magnetic-field-dependent Hall resistance (R_{xy}) loop. As shown in Figure 3c, the initial magnetization direction was at [110] crystal orientation (or 45°). A gradually increasing magnetic field was applied along [1−10] crystal orientation (or 315°). The Hall resistance rapidly changed from low to high states. With decreasing magnetic field, the Hall resistance did not recover to low state but maintained in a high resistance state. The magnetization process from high resistance to low resistance states shows the same behavior (Figure 3d). The above process is highly repeatable.

Coincidentally, the current-control DW rotation along [1−10] and [110] crystal orientations are perfectly match with the peak and valley values of the PHE. Therefore, we have chosen these two orientations as high and low resistance states to design a prototype domain-wall-based magnetic random-access memory (DW-MARM) device. The schematic concept of the full-scale eight electrodes DW-MRAM is shown in SI Figure S5. The demonstration of a full-scale electrical controlled DW-MARM device still needs further studies because our manufacture technology does not fit the current density along [110] crystal orientation. Therefore, as shown in Figure 4a, we use six electrodes device with an in-plane pulse magnetic field to simulate the electrodes along [110] crystal orientation. Single LSMO thin film is used as the magnetic memory cell. The pulsed currents input from electrodes along [1−10] crystal orientations served as write circuit. Four terminal electrodes along [100] and [010] crystal orientations are used for read process. Due to this unique orientation/angle relationships, the write and read circuits are separated, which can effectively reduce the circuit interference.[2] As shown in Figure 4b, an in-plane pulse magnetic field of 100 mT along [1−10] crystal orientation was applied to realign the stripe DWs to high resistance ([1−10]) state. By applying a current density of 2×10^5 A/cm^2 along [1−10] crystal orientation at zero magnetic field, the stripe DWs were rotated to low resistance ([110]) state (Figure 4c). Such high/low resistance switching shows nonvolatile and highly repeatable PHE readouts (Figure 4d).

https://doi.org/10.1021/acsami.1c04724
ACS Appl. Mater. Interfaces 2021, 13, 23945−23950

CONCLUSIONS

In summary, room-temperature current-controlled DW rotation in LSMO thin film has been observed. This DWs realignment shows intrinsically nonvolatile behavior, which can be readout by PHE. A DW-MRAM prototype device has been proposed. This concept shows great potentials with advantages including field-free switching, simple material structure and insensitive readout to thermal effect. Furthermore, the LSMO stripe domain can be stabilized in nanoscale islands[26] with a high integration capability. This design can be further extended to a broad variety of DW-based magnetic materials in multistate memory or even neuron memristor devices.

EXPERIMRNTAL METHODS

Epitaxial Growth of $La_{0.67}Sr_{0.33}MnO_3$ (LSMO) Thin Films. The epitaxial LSMO thin films were grown on $LaAlO_3$ substrates by pulsed laser deposition. Stoichiometric targets were ablated by a KrF excimer laser (248 nm). During the growth, the substrate temperature was kept at 780 °C and the oxygen pressure was 25 Pa. The laser energy density and frequency were set as approximately ∼0.7 J cm^{-2} and 5 Hz, respectively. After the deposition, the films were in situ cooled down to room temperature at 1 atm of oxygen with a cooling rate of 5 °C min^{-1}.

High Angle Annular Dark field (HAADF) Scanning Transmission Electron Microscopy (STEM). The cross-sectional STEM specimen was thinned to less than 30 μm first by mechanical polishing and then we performed argon ion milling. The ion-beam milling was carried out using PIPS (model 691, Gatan Inc.) with the accelerating voltage of 3.5 kV until a hole was made. Low voltage milling was performed with accelerating voltage of 0.3 kV to remove the surface amorphous layer. The HAADF−STEM images were recorded at an aberration corrected FEI (Titan Cubed Themis G2) operated at 300 kV. The convergence semiangle for imaging is 30 mrad, the collection semiangles snap is 39−200 mrad. The fast scanning directions are perpendicular to the surface and interface while the slow scanning direction are parallel in order to minimize errors induced by the scanning noise and specimen drift, in order to minimize errors induced by the scanning noise and specimen drift. To further reduce the errors, multiple images were fast recorded with small dwell time and summed together after careful alignments, which were automatically done by the Velox software provided by the microscope manufacturer Thermo fisher Scientific.

Synchrotron X-ray Diffraction (XRD). X-ray diffraction has been measured at beamline 1W1A of Beijing Synchrotron Radiation Facility with X-ray wavelength of 1.54851 Å.

Magnetic Force Microscopy. Magnetic force microscopy (MFM) were carried out on a Digital Instruments Nanoscope-V Multimode AFM under ambient conditions. The surface topography and domain structures were imaged by a tapping-mode MFM using commercially available Co−Cr-coated Si tips (MESP, Bruker). The magnetization of the tip was controlled using an external magnet. During the measurements, typical scanning rate of the cantilever was 0.8 Hz.

ASSOCIATED CONTENT

Supporting Information

The Supporting Information is available free of charge at https://pubs.acs.org/doi/10.1021/acsami.1c04724.

Methods, crystal structure analysis, thermal effect analysis, spin orbital coupling effect in single layer LSMO, the schematic concept of the DW-MRAM and the pictures of the devices (PDF)

AUTHOR INFORMATION

Corresponding Authors

Jie Wang − *Department of Engineering Mechanics & Key Laboratory of Soft Machines and Smart Devices of Zhejiang Province, Zhejiang University, Hangzhou 310012, China;* orcid.org/0000-0001-7854-9376; Email: jw@zju.edu.cn

Kangkang Meng − *School of Materials Science and Engineering, University of Science and Technology Beijing, Beijing 100083, China*; Email: kkmeng@ustb.edu.cn

Jinxing Zhang − *Department of Physics, Beijing Normal University, Beijing, China;* orcid.org/0000-0001-8977-5678; Email: jxzhang@bnu.edu.cn

Authors

Shizhe Wu − *Department of Physics, Beijing Normal University, Beijing, China;* orcid.org/0000-0002-5424-6554

Yuelin Zhang − *Department of Physics, Beijing Normal University, Beijing, China*

Chengfeng Tian − *Department of Physics, Beijing Normal University, Beijing, China*

Jianyu Zhang − *Fert Beijing Institute, BDBC, School of Microelectronics, Beihang University, Beijing 100875, China*

Mei Wu − *International Center for Quantum Materials, School of Physics, Peking University, Beijing 100871, China*

Yu Wang − *Department of Engineering Mechanics & Key Laboratory of Soft Machines and Smart Devices of Zhejiang Province, Zhejiang University, Hangzhou 310012, China*

Peng Gao − *International Center for Quantum Materials, School of Physics, Peking University, Beijing 100871, China;* orcid.org/0000-0003-0860-5525

Haiming Yu − *Fert Beijing Institute, BDBC, School of Microelectronics, Beihang University, Beijing 100875, China;* orcid.org/0000-0002-3291-6713

Yong Jiang − *School of Materials Science and Engineering, University of Science and Technology Beijing, Beijing 100083, China;* orcid.org/0000-0003-2011-7241

Complete contact information is available at: https://pubs.acs.org/10.1021/acsami.1c04724

Author Contributions

The manuscript was written through contributions of all authors. All authors have given approval to the final version of the manuscript.

Notes

The authors declare no competing financial interest.

ACKNOWLEDGMENTS

J.Z. acknowledge the financial support from the National Natural Science Foundation of China (11974052), Beijing National Laboratory for Condensed Matter Physics, Beijing Natural Science Foundation (Z190008), and the Chinese Academy of Sciences Interdisciplinary Innovation Team. J.W. acknowledge the financial support from the National Natural Science Foundation of China (11972320). K.M. acknowledge the financial support from the National Natural Science Foundation of China (51971027).

REFERENCES

(1) Dieny, B.; Prejbeanu, I. L.; Garello, K.; Gambardella, P.; Freitas, P.; Lehndorff, R.; Raberg, W.; Ebels, U.; Demokritov, S. O.; Akerman, J.; Deac, A.; Pirro, P.; Adelmann, C.; Anane, A.; Chumak, A. V.;

Hirohata, A.; Mangin, S.; Valenzuela, S. O.; Cengiz Onbaşlı, M.; d' Aquino, M.; Prenat, G.; Finocchio, G.; Lopez-Diaz, L.; Chantrell, R.; Chubykalo-Fesenko, O.; Bortolotti, P. Opportunities and Challenges for Spintronics in the Microelectronics Industry. *Nat. Electron.* **2020**, *3*, 446−459.
(2) Brataas, A.; Kent, A. D.; Ohno, H. Current-induced Torques in Magnetic Materials. *Nat. Mater.* **2012**, *11*, 372−381.
(3) Prenat, G.; Jabeur, K.; Vanhauwaert, P.; Pendina, G. D.; Oboril, F.; Bishnoi, R.; Ebrahimi, M.; Lamard, N.; Boulle, O.; Garello, K.; Langer, J.; Ocker, B.; Cyrille, M.-C.; Gambardella, P.; Tahoori, M.; Gaudin, G. Ultra-fast and High-reliability SOT-MRAM: From Cache Replacement to Normally-off Computing. *IEEE Transactions on Multi-Scale Computing Systems* **2016**, *2*, 49−60.
(4) Gambardell, P.; Miron, I. M.; Trans, P. Current-induced Spin-orbit Torques. *Philos. Trans. R. Soc., A* **2011**, *369*, 3175−3197.
(5) Manchon, A.; Koo, H. C.; Nitta, J.; Frolov, S. M.; Duine, R. A. New Perspectives for Rashba Spin-orbit Coupling. *Nat. Mater.* **2015**, *14*, 871−882.
(6) Miron, I. M.; Garello, K.; Gaudin, G.; Zermatten, P.-J.; Costache, M. V.; Auffret, S.; Bandiera, S.; Rodmacq, B.; Schuhl, A.; Gambardella, P. Perpendicular Switching of a Single Ferromagnetic Layer Induced by In-plane Current Injection. *Nature* **2011**, *476*, 189−193.
(7) Liu, L.; Pai, C.-F.; Li, Y.; Tseng, H. W.; Ralph, D. C.; Buhrman, R. A. Spin-torque Switching with the Giant Spin Hall Effect of Tantalum. *Science* **2012**, *336*, 555−558.
(8) Meng, K. K.; Miao, J.; Xu, X. G.; Wu, Y.; Zhao, X. P.; Zhao, J. H.; Jiang, Y. Anomalous Hall effect and Spin-orbit Torques in MnGa/IrMn Films: Modification From Strong Spin Hall Effect of the Antiferromagnet. *Phys. Rev. B: Condens. Matter Mater. Phys.* **2016**, *94*, 214413.
(9) Liu, L.; Qin, Q.; Lin, W.; Li, C.; Xie, Q.; He, S.; Shu, X.; Zhou, C.; Lim, Z.; Yu, J.; Lu, W.; Li, M.; Yan, X.; Pennycook, S. J.; Chen, J. Current-induced Magnetization Switching in All-oxide Heterostructures. *Nat. Nanotechnol.* **2019**, *14*, 939−944.
(10) Chernyshov, A.; Overby, M.; Liu, X.; Furdyna, J. K.; Lyanda-Geller, Y.; Rokhinson, L. P. Evidence for Reversible Control of Magnetization in a Ferromagnetic Material by means of Spin−orbit Magnetic Field. *Nat. Phys.* **2009**, *5*, 656−659.
(11) Bodnar, S. Yu.; šmejkal, L.; Turek, I.; Jungwirth, T.; Gomonay, O.; Sinova, J.; Sapozhnik, A. A.; Elmers, H.-J.; Kläui, M.; Jourdan, M. Writing and Reading Antiferromagnetic Mn_2Au by Néel Spin-orbit Torques and Large Anisotropic Magnetoresistance. *Nat. Commun.* **2018**, *9*, 348.
(12) Meinert, M.; Graulich, D.; Matalla-Wagner, T. Electrical Switching of Antiferromagnetic Mn_2Au and the Role of Thermal Activation. *Phys. Rev. Appl.* **2018**, *9*, 064040.
(13) Jiang, M.; Asahara, H.; Sato, S.; Kanaki, T.; Yamasaki, H.; Ohya, S.; Tanaka, M. Efficient Full Spin−orbit Torque Switching in a Single Layer of a Perpendicularly Magnetized Singlecrystalline Ferromagnet. *Nat. Commun.* **2019**, *10*, 2590.
(14) Miron, I. M.; Gaudin, G.; Auffret, S.; Rodmacq, B.; Schuhl, A.; Pizzini, S.; Vogel, J.; Gambardella, P. Current-driven Spin Torque Induced by the Rashba Effect in a Ferromagnetic Metal Layer. *Nat. Mater.* **2010**, *9*, 230−234.
(15) Fin, S.; Tomasello, R.; Bisero, D.; Marangolo, M.; Sacchi, M.; Popescu, H.; Eddrief, M.; Hepburn, C.; Finocchio, G.; Carpentieri, M.; Rettori, A.; Pini, M. G.; Tacchi, S. In-plane Rotation of Magnetic Stripe Domains in $Fe_{1-x}Ga_x$ Thin Films. *Phys. Rev. B: Condens. Matter Mater. Phys.* **2015**, *92*, 224411.
(16) Bakaul, S. R.; Hu, W.; Wu, T.; Kimura, T. Intrinsic Domain-wall Resistivity in Half-metallic Manganite Thin Films. *Phys. Rev. B: Condens. Matter Mater. Phys.* **2012**, *86*, 184404.
(17) Liu, C.; Wu, S. Z.; Zhang, J. Y.; Chen, J. L.; Ding, J. J.; Ma, J.; Zhang, Y. L.; Sun, Y. W.; Tu, S.; Wang, H. C.; Liu, P. F.; Li, C. X.; Jiang, Y.; Gao, P.; Yu, D. P.; Xiao, J.; Duine, R.; Wu, M. Z.; Nan, C. W.; Zhang, J. X.; Yu, H. M. Current-controlled Propagation of Spin Waves in Antiparallel, Coupled Domains. *Nat. Nanotechnol.* **2019**, *14*, 691−697.
(18) Wang, J.; Xie, L. S.; Wang, C. S.; Zhang, H. Z.; Shu, L.; Bai, J.; Chai, Y. S.; Zhao, X.; Nie, J. C.; Cao, C. B.; Gu, C. Z.; Xiong, C. M.; Sun, Y.; Shi, J.; Salahuddin, S.; Xia, K.; Nan, C. W.; Zhang, J. X. Magnetic Domain-wall Motion Twisted by Nanoscale Probe-induced Spin Transfer. *Phys. Rev. B: Condens. Matter Mater. Phys.* **2014**, *90*, 224407.
(19) Legrand, W.; Chauleau, J.-Y.; Maccariello, D.; Reyren, N.; Collin, S.; Bouzehouane, K.; Jaouen, N.; Cros, V.; Fert, A. Hybrid Chiral Domain Walls and Skyrmions in Magnetic Multilayers. *Sci. Adv.* **2018**, *4*, No. eaat0415.
(20) Yamanouchi, M.; Oyamada, T.; Ohta, H. Peculiar Magneto-transport Properties in $La_{0.67}Sr_{0.33}MnO_3/LaAlO_3/SrTiO_3$. *AIP Adv.* **2019**, *9*, 035129.
(21) Yamanouchi, M.; Oyamada, T.; Ohta, H. Current-induced Effective Magnetic Field in $La_{0.67}Sr_{0.33}MnO_3/LaAlO_3/SrTiO_3$ Structures. *AIP Adv.* **2020**, *10*, 015129.
(22) Wang, J.; Wu, S. Z.; Ma, J.; Xie, L. S.; Wang, C. S.; Malik, I. A.; Zhang, Y. L.; Xia, K.; Nan, C.-W.; Zhang, J. X. Nanoscale Control of Stripe-ordered Magnetic Domain Walls by Vertical Spin Transfer Torque in $La_{0.67}Sr_{0.33}MnO_3$ Film. *Appl. Phys. Lett.* **2018**, *112*, 072408.
(23) Tang, H. X.; Kawakami, R. K.; Awschalom, D. D.; Roukes, M. L. Giant Planar Hall Effect in Epitaxial (Ga,Mn)As Devices. *Phys. Rev. Lett.* **2003**, *90*, 107201.
(24) Nandy, S.; Sharma, G.; Taraphder, A.; Tewari, S. Chiral Anomaly as the Origin of the Planar Hall Effect in Weyl Semimetals. *Phys. Rev. Lett.* **2017**, *119*, 176804.
(25) Montaigne, F.; Schuhl, A.; Van Dau, F. N.; Encinas, A. Development of Magnetoresistive Sensors Based on Planar Hall Effect for Applications to Microcompass. *Sens. Actuators, A* **2000**, *81*, 324−327.
(26) Wu, Y.; Matsushita, Y.; Suzuki, Y. Nanoscale Magnetic-domain Structure in Colossal Magnetoresistance Island. *Phys. Rev. B: Condens. Matter Mater. Phys.* **2001**, *64*, 220404.

https://doi.org/10.1021/acsami.1c04724
ACS Appl. Mater. Interfaces 2021, 13, 23945−23950